The application of the Lattice Boltzmann Method in the calculation of the virtual mass

Nastaran Ahmadpour Samani Ali Moradi Britt M. E. Moldestad

Department of Process, Energy and Environmental Technology, University of South-Eastern Norway,
nastaran.samani@usn.no
ali.moradi@usn.no
britt.moldestad@usn.no

Abstract

Virtual mass is an important quantity in the analysis of the unsteady motion of objects underwater or other fluids or unsteady flow around bodies, for example, the virtual mass effect is important in the inertia of ships, floaters, swimmers' organs, airplanes, and bubbles. The additional mass resulting from the fluid acting on the structure can be calculated by solving the equation of potential flow around the object. In this paper, a system in which a square object is immersed in a channel of fluid and moves parallel to the wall has been considered. The corresponding virtual mass at a determined distance $\boldsymbol{S}$ from the wall and for the object size $\boldsymbol{D}$ (the side of the square object) is calculated via the Lattice Boltzmann Method. Here, it is tried to change $\boldsymbol{D}$ and $\boldsymbol{S}$ separately and investigate their effects on the virtual mass. According to the simulation results, for the systems in which the distance from the wall is more than four times the object size ($\boldsymbol{S} > 4\boldsymbol{D}$), the distance does not influence the added mass. Furthermore, the virtual mass rises when the object approaches the wall and experiences its maximum value as it reaches the wall ($\boldsymbol{S} \rightarrow \boldsymbol{0}$). As a result, in this case, the virtual mass is about 75% larger than in the case of $\boldsymbol{S}=4\boldsymbol{D}$. In addition, the simulations reveal that by increasing the dimensions of the object $\boldsymbol{D}$ the virtual mass increases and vice versa.

Keywords: Lattice Boltzmann simulation, added/virtual mass, variable size, various distance, bounce-back boundary condition

1 Introduction

The Lattice Boltzmann Method (LBM) which is a mesoscopic method based on simplified kinetic equations, has been significantly taken into consideration in classical statistical physics. LBM can be an appropriate alternative approach to the current finite difference, finite element, and finite volume techniques for solving the Navier Stokes equations. According to this method, it has been concluded that if only collective macroscopic flow behavior is investigated, the macroscopic behavior of a fluid system is generally not very sensitive to the underlying microscopic behavior of the particle. In LBM, the simulation is based on the modeling of fluid flow as a collection of particles colliding over a discrete lattice sphere. In this method, the Boltzmann equation is solved on a discrete lattice and instead of solving Navier Stokes equations, the density of the fluid is simulated during two steps including streaming and collision. Owing to its underlying kinetic property, the ability to combine microscopic interactions, and using bounce back boundary conditions, the LBM has been increasingly applied in the simulation of fluid flow especially interfacial dynamics and complicated boundaries and geometries, such as multiphase/multicomponent flows in porous media (Hinebaugh et al., 2012; Tu et al., 2018; Succi, 2001). The Lattice Boltzmann Method has been used in the simulation of a wide variety of fluid dynamical applications. The method is really practical in the simulation of turbulent single-phase flow, flow in porous media, and multiphase flows in several industrial applications (Chen and Doolen, 1998). LBM has been applied in various simulations such as flow in porous media (Pan et al., 2006; Nabovati et al., 2009), colloidal suspensions (Kutay et al., 2006), multiphase and multicomponent flows (Yang and Boek, 2013; Inamuro et al., 2004), and several other applications.

In this study, the additional mass of a two-dimensional object is simulated using the Lattice Boltzmann Method. Numerous forces are exerted on a body moving in a fluid. Lift and drag forces are exerted on bodies in a fluid due to surface friction and the variation of pressure around the bodies. In order for a moving body to move in a fluid, it must counteract the fluid and move it. Therefore, not only should the body move its weight, but it should also move the surrounding fluid. Hence, to counteract the fluid's inertia, the body faces additional forces, and it senses further weight than that of its weight. If the density of the body is greater than that of the fluid, the additional force can be overlooked. Otherwise, it must be considered. The additional force which is caused by the fluid inertia is called added mass. Other titles such as virtual mass, hydrodynamic mass, effective mass, inertial mass, apparent mass, and induced mass are also applied. The calculation of virtual mass is a challenging procedure in the analysis of bodies moving in the water.

In (Cebeci et al., 2005) the low-speed unsteady airfoils were investigated by researchers, and it was demonstrated that further forces are exerted on airfoils in moving fluids. Additional mass for various geometries was calculated by employing the complex function methods by Korotkin (Korotkin, 2008). The value of the body acceleration did not have any effect on the value of additional mass (Wakaba and Balachandar, 2007). The additional mass for various figures in low-depth water was calculated (Zhou et al., 2005). The additional mass for a cylinder which was placed between two parallel plates was measured by Kharlamov (Kharlamov, 2012). The additional mass for a hydrofoil with cavitation was calculated by Benaouicha (Benaouicha et al., 2012). Investigated vibration characteristic of a thin layer in the air by implementing empirical methods was studied in (Yuanqi et al., 2011). Furthermore, the additional mass for a swimmer, the effects of deformation, and the size of a swimmer, i.e. a man or a woman were studied by Caspersen (Caspersen et al., 2010). The influence of additional mass on the forces exerted on insect wings was studied by Yan (Yan et al., 2011). Guo investigated the added mass effect of seawater on pipeline vibration (Guo et al., 2013).

In this investigation, initially, the additional mass for a body when it is far from a wall is calculated and it is compared with the exact results. Afterward, the effects of the wall near the body on additional mass are investigated. Moreover, the dimensions of the deformed body and its effects on the additional mass are taken into consideration.

2 Fundamental equations

Figure 1 presents the investigated problem of this study, which is a square body with dimensions that moves parallel to the wall. In order to determine the additional mass, potential fluid around the body is considered. Laplacian equation for the potential equation is as follows (Versteeg and Malalasekera, 2007):

$$\frac{\partial^2 \varphi}{\partial x^2}+\frac{\partial^2 \varphi}{\partial y^2}=0 \qquad (1)$$

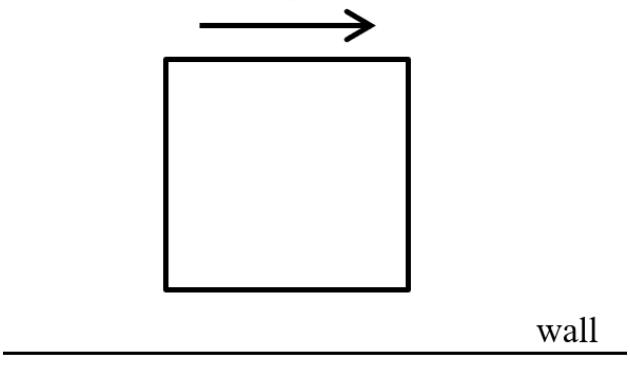

Figure 1. Figure of square moving body

It is feasible to assume that the fluid is moving instead of the body. Boundary conditions are depicted in Figure 2. For a uniform potential fluid flow in the *x*-direction, the potential function changes linearly with *x*. The gradient of the potential function in the direction of perpendicular on the surface for the wall, the body, and the top boundary condition is equal to zero. The value of the potential equation is assumed for the right and left boundaries, which are zero, and φ_0 for the left and right boundaries, respectively. The length of the solution must be considered in a way that satisfies $\partial\varphi/\partial y$ and $\partial\varphi/\partial x$ in the regions which are near the wall boundaries. In fact, the amplitude of the solution should be chosen so that integration on the solution amplitude yields the proper results. The dimensions of solution amplitude are represented in Figure 3. The distance between the body and the wall is specified by *S* and 9*D* is the length of the solution range. The accuracy of the presented dimensions is investigated in the results section. The dimensionless parameters are defined as (Mohamad, 2011):

$$Y\equiv\frac{y}{D} \qquad \phi=\frac{\varphi}{\varphi_0}\frac{L}{D} \qquad U\equiv\frac{uL}{\varphi_0} \qquad \mathrm{X}\equiv\frac{x}{D} \qquad \phi=\frac{T-100}{100} \qquad (2)$$

L is the solution amplitude.

$$\frac{\partial^2 \phi}{\partial X^2}+\frac{\partial^2 \phi}{\partial Y^2}=0 \qquad (3)$$

$$\phi(\frac{+L}{2},X)=\frac{L}{D} \qquad \phi(\frac{-L}{2},Y)=0 \qquad (4)$$

On the top and bottom boundary:

$$\frac{\partial \phi}{\partial Y}=0$$

And on the body:

$$\frac{\partial \phi}{\partial n}=0$$

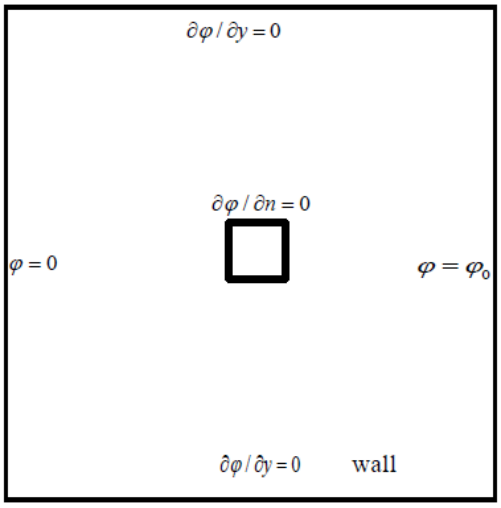

Figure 2. Boundary conditions

Based on the 2D or 3D body dimensions, the additional mass has numerous components. In this study, a two-dimensional body with one-dimensional moving and one component additional mass is taken into account. Additional mass is going to be dimensionless regarding the following equation.

$$M = \frac{m}{\rho D^2} \tag{5}$$

The mass, m [kg/m] is defined as the additional mass of the object at a specified distance from the wall. ρ [kg/m^3] is fluid density and D [m] is the distance from the wall.

After determining the potential equation, the value of additional mass is calculated from (Graebel 2007):

$$M = \iint M_{11}(X,Y)\,dX\,dY \tag{6}$$

$$M_{11}(X,Y) = \left(\frac{\partial \phi}{\partial X} - 1\right)^2 + \left(\frac{\partial \phi}{\partial Y}\right)^2 \tag{7}$$

In contrast to regions near the body, the value of $M_{11}(X, Y)$ is zero in regions far from the body.

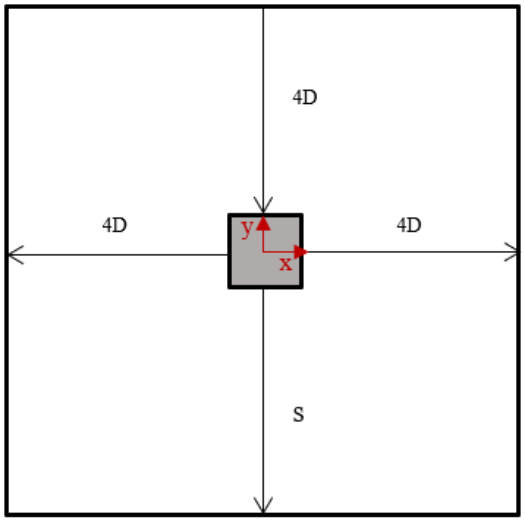

Figure 3. Dimensions of solution amplitude

3 Boltzmann Method

The Boltzmann procedure is explained by Mohamad (Mohamad, 2011). The solution amplitude is divided into nodes of equal size. D_2Q_9 is implemented in this study and the $g(i)$ distribution equation is employed. The following correlation is governed for the $g(i)$ equations (Mohamad, 2011):

$$g_i(\vec{r} + \vec{e}_i \delta t, t + \delta t) = g_i + \frac{g_i^{eq} - g_i}{\tau} \tag{8}$$

$\vec{r}$ is the position vector of a node, τ is the relaxation time, and g_i^{eq} is the vector of the distribution equation. $\vec{e}_i$ vectors are depicted in Figure 4 and its value is as follows. In addition, g_i^{eq} is presented as (Mohamad, 2011):

$$\left\|\vec{e}_0\right\| = 0, \qquad \left\|\vec{e}_{1,2,3,4}\right\| = 1, \qquad \left\|\vec{e}_{5,6,7,8}\right\| = \sqrt{2} \tag{9}$$

$$\left\{ \begin{array}{l} g_0^{eq} = 0 \\ g_1^{eq} = g_2^{eq} = g_3^{eq} = g_4^{eq} = \frac{1}{6}\phi \\ g_5^{eq} = g_6^{eq} = g_7^{eq} = g_8^{eq} = \frac{1}{12}\phi \end{array} \right\} \tag{10}$$

Boltzmann correlation is solved at the two stages of collision and stream (Mohamad, 2011):

$$g_i(\vec{r}, t + \delta t) = g_i + \frac{g_i^{eq} - g_i}{\tau} \tag{11}$$

$$g_\alpha\left(\vec{r} + \vec{e}_i t, t + \delta t\right) = g_\alpha\left(\vec{r}, t + \delta t\right) \tag{12}$$

At the collision stage, Equation 11, the values of distribution equations are calculated from the previous stage. Each node at the stream stage transfers to another node in the opposite direction.

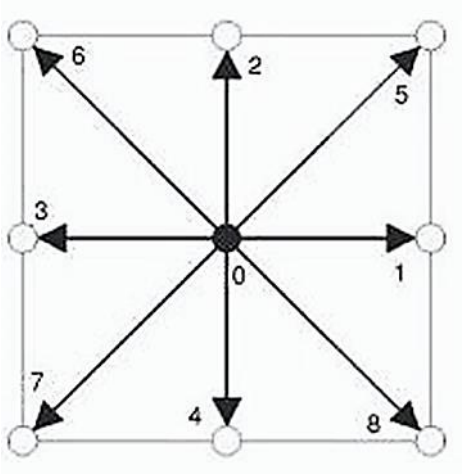

Figure 4. D2Q9 Lattice model

After the determination of the distribution equation in each node, the value of the potential equation and its derivatives are determined as follows (Mohamad, 2011);

$$\phi = \sum_{i=0}^{8} g_i \tag{13}$$

$$\vec{\nabla}\phi = \frac{\tau - 0.5}{\tau} \sum_{i=0}^{8} \vec{e}_i g_i \tag{14}$$

At the stream stage, no value is transferred to the distribution equations, i.e., $g(i)$ on the boundaries. There are three paths on each node, in which no value is transferred to them so that the boundary conditions for these nodes can determine the distribution functions on unknown nodes. For example, the values of g_3, g_6, and g_7 are unknown for the right boundary because there is no node after the right boundary to transfer the values

based on Equation 12 to these functions. The value of the potential equation is known for the right boundary ($\varphi_R \equiv L/D$):

$$\varphi_R = g_0 + g_1 + ... + g_8 \quad (15)$$

The value of the potential equation is constant at the direction of this boundary and hence the potential equation is zero in this direction:

$$\frac{\partial \phi}{\partial Y} = \frac{\tau - 0.5}{\tau}(g_2 + g_6 + g_5 - g_4 - g_7 - g_8) = 0 \quad (16)$$

According to the bounce-back condition, the value of the distribution equation is equal for the directions normal to the boundary, thus for the right boundary:

$$g_3 = g_1 \quad (17)$$

From Equations 15 and 16, it is concluded that:

$$g_6 = \frac{\phi_R}{2} - (\frac{g_0}{2} + g_1 + g_2 + g_5) \quad (18)$$

$$g_7 = \frac{\phi_R}{2} - (\frac{g_0}{2} + g_1 + g_4 + g_8) \quad (19)$$

The procedure for the left boundary is the same as the right boundary.

The values of g_4, g_7, and g_8 are unknown for the top boundary. This is due to the fact that on this boundary $\frac{\partial \varphi}{\partial y} = 0$, and Equation 16 is accurate if:

$$g_4 = g_2, \qquad g_7 = g_6, \qquad g_8 = g_5 \quad (20)$$

Therefore, the value of *g(i)* which is unknown for the nodes is equal to its symmetry concerning the boundary. The current method is used for the bottom boundary and the outer of the body. For the entire calculations in this study $\tau = 1.5$ is assumed. The procedure of solving is started with an initial condition by assuming the value φ is zero for every node. Afterward, this procedure continues until the variations of φ or M become insignificant between two-time steps.

4 Results

In this contribution, the value of additional mass for a square body that is placed far from a wall is initially investigated, and in this case, *M*=1.189 is deduced. The problem is solved for the various node distances in order to determine the best number of nodes. The effect of node number on the value of additional mass is presented in Table 1. Regarding the presented relative error on the table, the distance between the nodes has been chosen to be 1/69. The number of nodes is 630×630.

Table 1. The influence of the number of nodes on added mass

ΔX	M	$E\%$
1/9	2.225	87
1/19	1.448	22
1/29	1.300	9.32
1/39	1.246	4.8
1/49	1.219	2.5
1/59	1.204	1.3
1/69	1.195	0.5

The constant potential lines and M_{11} distribution are presented in Figure 5. The potential equation at the places far from the body is linear, and the velocity reaches its final constant value. According to the horizontal moving of the body, the M_{11} variations are higher at the front and back sides of the body.

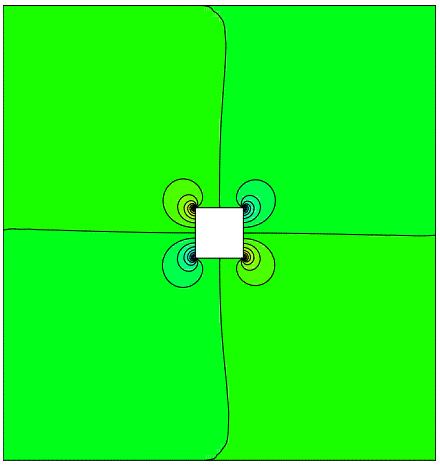

Figure 5. M_{11} distribution, for dimension of D×D and S=4D

Figure 6 represents potential lines and M_{11} distribution for the case in which the body is approaching the wall and *S=D*. By approaching the wall, the displacement of the body is going to be more complicated, and this is due to an additional mass increase in the regions near the wall. The problem is solved for *S/D*= 4, 3, 2, 1, 0.75, 0.5, 0.25, 0. The variation of additional mass versus the distance from the wall is shown in Figure 7. By approaching the wall, the value of additional mass increases, and its value increased by approximately 75% as the body reach the wall. The diagram of Figure 7 can be expanded by applying Equation 21. The equation has been achieved by curve fitting in MATLAB.

$$M = 0.857\, e^{(-3.2(S/D)+1.182)} \quad (17)$$

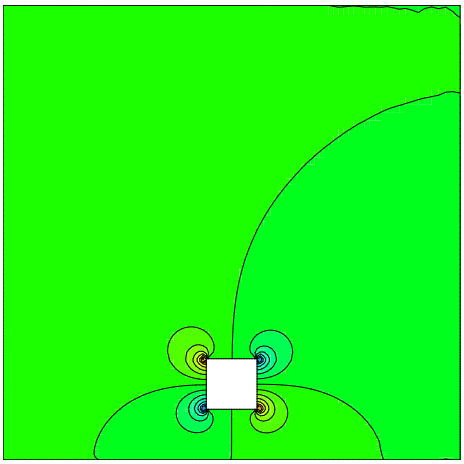

Figure 6. M_{11} distribution, for dimension of D×D and S=D

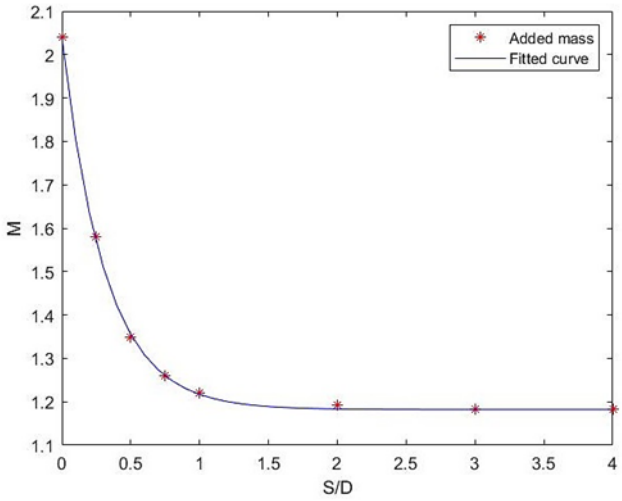

Figure 7. The variation of additional mass versus the distance from the wall

Moreover, the dimensions of the body have been changed and its influences upon additional mass are calculated. Constant potential lines and M_{11} distribution are presented in Figure 8 for a body with $0.8D\times D$ dimensions. Figure 9 demonstrates potential lines and M_{11} distribution for a case in which the body approaches the wall, i.e., $S=D$. By approaching the wall, body displacements become much harder, and this is because of the additional mass increase near the wall. The problem is solved for S/D= 4, 3, 2, 1, 0.75, 0.5, 0.25, 0. It is concluded that additional mass decreases by the decrease in the dimensions of the body.

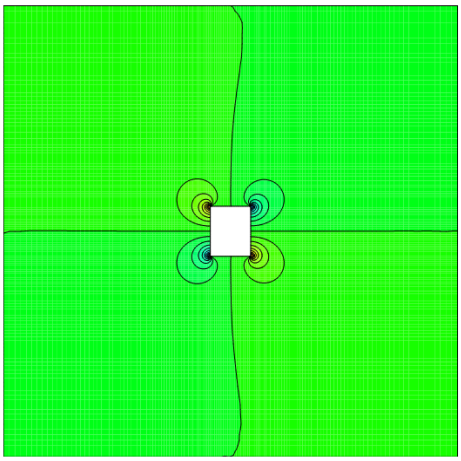

Figure 8. M_{11} distribution for dimension of 0.8D×D and S=4D

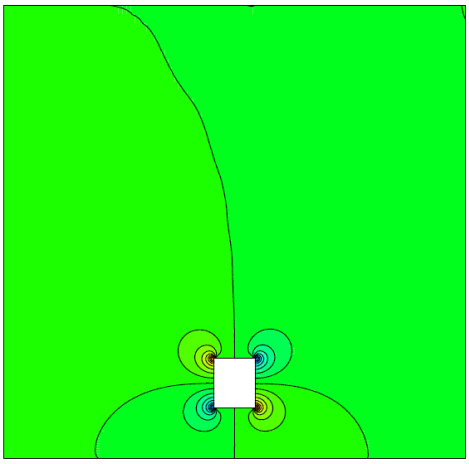

Figure 9. M_{11} distribution, for size of 0.8D×D and S=D

Figure 10 shows constant potential lines and M_{11} distribution for a body with $1.2D\times D$ dimensions. Figure11 shows potential lines and M_{11} distribution for a case in which the body approaches the wall, i.e. $S=D$. The displacement of the body becomes much more complicated as the body approaches the wall, and this is because of the increase in the values of additional mass in the regions near the wall. The problem is considered by determining S/D= 4, 3, 2, 1, 0.75, 0.5, 0.25, 0, and it is concluded that additional mass increases by increasing the dimensions of the body.

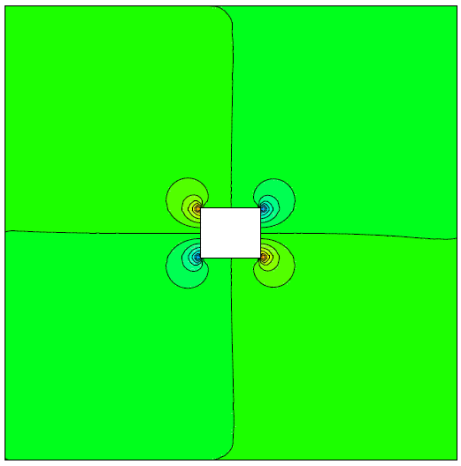

Figure 10. M_{11} distribution, for dimension of 1.2D×D and S=4D

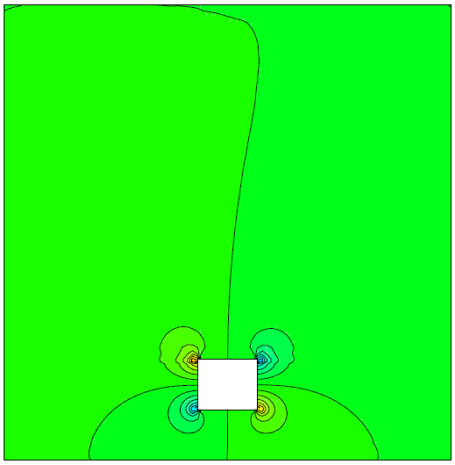

Figure 11. M_{11} distribution, for the dimension of 1.2D×D and S=D

The added masses of the body in the different dimensions in the distance equal to 4*D* from the wall have been validated by the results by Korotkin, in 2008. The results in Table 2 revealed that the added masses calculated by the Lattice Boltzmann Method have a very good constancy with the results in (Korotkin, 2008). The deviation between measured added masses and data in (Korotkin, 2008) varies between 0.9 % and 5 %, and the root mean square error is 2 %.

Table 2. Validation of the calculated added mass from Lattice Boltzmann Method for different dimensions in the distance equal to 4D from the wall with the results in (Korotkin, 2008)

Dimensions	*M_calculated [kg]*	*M (Korotkin 2008) [kg]*
0.4D×D	1.053	1.115
0.8D×D	1.148	1.162
D×D	1.182	1.193
1.2D×D	1.211	1.23
1.4D×D	1.234	1.257
1.6D×D	1.254	1.28
1.8D×D	1.27	1.304
2D×D	1.284	1.327

Furthermore, this procedure is employed for the cases in which the dimensions of the body are 2*D*×*D*, 1.8*D*×*D*, 1.6*D*×*D*, and 1.4*D*×*D*, and the value of additional mass is calculated. Figure 12 represents the variations of the calculated added masses of a body with various dimensions at different distances from the wall. Figure 13 shows the effects of the dimension of the body on the calculated added mass.

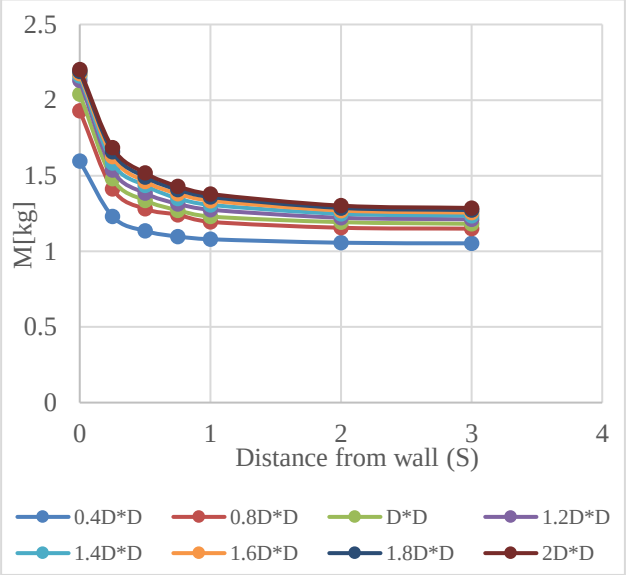

Figure 12. The variation of added masses of different sizes of body versus distance from the wall

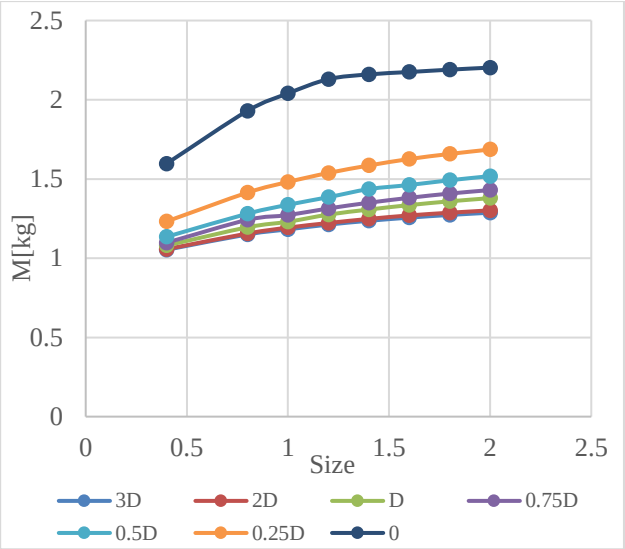

Figure 13. The variation of virtual masses of a body in different distances of the wall versus the dimension of the body

5 Conclusion

Added mass is an important quantity in the analysis of the motion of a submerged object, for example, ships crossing canals. The added mass increases when the object approaches the wall and reaches its maximum value as it moves on the wall ($\boldsymbol{S \rightarrow 0}$). In this case, the added mass is about 75% larger than for the case with $\boldsymbol{S}$=4$\boldsymbol{D}$. In addition, it is observed that the added mass increases by an increase of the object size $\boldsymbol{D}$ and vice versa. By increasing the size of the object to twice, the amount of added mass enhances between 8 to 15% depending on the distance of the object from the wall. The results of the measured added mass using the Lattice Boltzmann Method at the distance of 4D from the wall were validated with the results in the book by Korotkin and the results have a good consistency (RMSE =2%).

References

Mustapha Benaouicha, and Jacques-André Astolfi. Analysis of added mass in cavitating flow. *Journal of fluids and structures.* 31:30-48, 2012.

Cecilie Caspersen, Petter A. Berthelsen, Mari Eik, Csaba Pâkozdi, and Per-Ludvik Kjendlie. Added mass in human swimmers: age and gender differences. *Journal of Biomechanics*. 43, no. 12: 2369-2373, 2010.

Tuncer Cebeci, Max Platzer, Hsun Chen, Kuo-Cheng Chang, and Jian P. Shao. *Analysis of low-speed unsteady airfoil flows*. Springer Berlin Heidelberg, 2005.

Shiyi Chen, and Gary D. Doolen. Lattice Boltzmann method for fluid flows. *Annual review of fluid mechanics*. 30, no. 1: 329-364, 1998.

William Graebel. *Advanced fluid mechanics*. Academic Press, 2007.

Boyun Guo, Shanhong Song, Ali Ghalambor, and Tian Ran Lin. *Offshore pipelines: design, installation, and maintenance*. Gulf Professional Publishing, 2013.

J. Hinebaugh, A. Bazylak, and P. P. Mukherjee. Multi-scale modeling of two-phase transport in polymer electrolyte membrane fuel cells. *Polymer electrolyte membrane and direct methanol fuel cell technology*. pp. 254-292e. Woodhead Publishing, 2012.

Takaji Inamuro. Lattice Boltzmann methods for moving boundary flows. *Fluid Dynamics Research* 44. no. 2: 024001, 2012.

A. A. Kharlamov. The virtual mass coefficients of a circular cylinder moving in an ideal fluid between parallel walls. *Journal of Applied Mathematics and Mechanics*. 76, no. 1: 98-102, 2012.

Alexandr I. Korotkin. *Added masses of ship structures*. Vol. 88. Springer Science & Business Media, 2008.

Muhammed E. Kutay, Ahmet H. Aydilek, and Eyad Masad. Laboratory validation of lattice Boltzmann method for modeling pore-scale flow in granular materials. *Computers and Geotechnics* 33, no. 8 (2006): 381-395.

A. A. Mohamad. *Lattice Boltzmann Method*. Vol. 70. London: Springer, 2011.

Aydin Nabovati, Edward W. Llewellin, and Antonio CM Sousa. A general model for the permeability of fibrous porous media based on fluid flow simulations using the lattice Boltzmann method. *Composites Part A: Applied Science and Manufacturing* 40, no. 6-7: 860-869, 2009.

Chongxun Pan, Li-Shi Luo, and Cass T. Miller. An evaluation of lattice Boltzmann schemes for porous medium flow simulation. *Computers & fluids* 35, no. 8-9: 898-909, 2006.

Sauro Succi. *The lattice Boltzmann equation: for fluid dynamics and beyond*. Oxford university press, 2001.

Jiyuan Tu, Guan Heng Yeoh, and Chaoqun Liu. *Computational fluid dynamics: a practical approach*. Butterworth-Heinemann, 2018.

Henk Kaarle Versteeg, and Weeratunge Malalasekera. *An introduction to computational fluid dynamics: the finite volume method*. Pearson education, 2007.

Y. J. Lee, Kim-Boon Lua, T. T. Lim, and K. S. Yeo. A quasi-steady aerodynamic model for flapping flight with improved adaptability. *Bioinspiration & biomimetics* 11, no. 3: 036005, 2016.

L. Wakaba, and S. Balachandar. On the added mass force at finite Reynolds and acceleration numbers. *Theoretical and Computational fluid dynamics* 21, no. 2: 147-153, 2007.

Xingyao Yan, Shanan Zhu, Zhongdi Su, and Hongjun Zhang. Added mass effect and an extended unsteady blade element model of insect hovering. *Journal of Bionic Engineering* 8, no. 4: 387-394, 2011.

Jianhui Yang, and Edo S. Boek. A comparison study of multi-component Lattice Boltzmann models for flow in porous media applications. *Computers & Mathematics with Applications* 65, no. 6: 882-890, 2013.

Li Yuanqi, Lei Wang, Zuyan Shen, and Yukio Tamura. Added-mass estimation of flat membranes vibrating in still air. *Journal of Wind Engineering and Industrial Aerodynamics* 99, no. 8: 815-824, 2011.

Z. X. Zhou, Edmond YM Lo, and S. K. Tan. Effect of shallow and narrow water on added mass of cylinders with various cross-sectional shapes. *Ocean engineering* 32, no. 10: 1199-1215, 2005.